Stem Cell Reports
Article
ISSCR
OPEN ACCESS

Intrinsically Active and Pacemaker Neurons in Pluripotent Stem Cell-Derived Neuronal Populations

Sebastian Illes,[1,2] Martin Jakab,[3] Felix Beyer,[4] Renate Gelfert,[1,2] Sébastien Couillard-Despres,[1,2,5] Alfons Schnitzler,[4] Markus Ritter,[3] and Ludwig Aigner[1,2,*]
[1]Institute of Molecular Regenerative Medicine, Paracelsus Medical University, 5020 Salzburg, Austria, Austria
[2]Spinal Cord Injury and Tissue Regeneration Center Salzburg (SCI-TReCS), Salzburg, Paracelsus Medical University, 5020 Salzburg, Austria
[3]Institute of Physiology and Pathophysiology, Paracelsus Medical University, 5020 Salzburg, Austria
[4]Institute of Clinical Neuroscience and Medical Psychology, Heinrich Heine University Düsseldorf, 40225 Düsseldorf, Germany
[5]Institute of Experimental Neuroregeneration, Paracelsus Medical University, 5020 Salzburg, Austria
*Correspondence: ludwig.aigner@pmu.ac.at
http://dx.doi.org/10.1016/j.stemcr.2014.01.006

SUMMARY

Neurons generated from pluripotent stem cells (PSCs) self-organize into functional neuronal assemblies in vitro, generating synchronous network activities. Intriguingly, PSC-derived neuronal assemblies develop spontaneous activities that are independent of external stimulation, suggesting the presence of thus far undetected intrinsically active neurons (IANs). Here, by using mouse embryonic stem cells, we provide evidence for the existence of IANs in PSC-neuronal networks based on extracellular multielectrode array and intracellular patch-clamp recordings. IANs remain active after pharmacological inhibition of fast synaptic communication and possess intrinsic mechanisms required for autonomous neuronal activity. PSC-derived IANs are functionally integrated in PSC-neuronal populations, contribute to synchronous network bursting, and exhibit pacemaker properties. The intrinsic activity and pacemaker properties of the neuronal subpopulation identified herein may be particularly relevant for interventions involving transplantation of neural tissues. IANs may be a key element in the regulation of the functional activity of grafted as well as preexisting host neuronal networks.

INTRODUCTION

Spontaneous neuronal activity refers to the ability of an individual neuron or an entire neuronal network to be electrophysiologically active without receiving external stimulation. Such spontaneous activity is present in both the developing and the adult brain (Blankenship and Feller, 2010; de Pasquale et al., 2010; Liu et al., 2010). Also, isolated brain slices (i.e., segments of brain that are deprived of input from other brain regions) show spontaneous neuronal activities (Darbon et al., 2002a; Le Bon-Jego and Yuste, 2007; Shew et al., 2010), and dissociated neuronal cells self-organize into spontaneously spiking or synchronously bursting neuronal networks in vitro (Arnold et al., 2005; Streit et al., 2001; Van Pelt et al., 2004). Autonomous network activities rely on neurons, which are able to be spontaneously active even in conditions where fast synaptic communication (FSC) has been silenced. These neurons have therefore been termed intrinsically active neurons (IANs). IANs can be found in nearly all brain regions that have been investigated to date (Atherton and Bevan, 2005; Atherton et al., 2008; Beatty et al., 2012; Mao et al., 2001; Streit et al., 2001; Tazerart et al., 2008), where they act as pacemaker neurons in regulating oscillatory activities in neuronal assemblies (Beatty et al., 2012; Feldman and Del Negro, 2006; Le Bon-Jego and Yuste, 2007; Tazerart et al., 2008; Tscherter et al., 2001). Thus, IANs represent key neuronal elements that spontaneously induce activities in other neurons, and may regulate different types of orchestrated activities in neuronal assemblies. Moreover, the ability of neurons to self-organize into functional neuronal networks generating oscillatory neuronal activities is crucial for proper cognitive as well as motor functions.

Multielectrode array (MEA) recordings and calcium imaging of human and murine pluripotent stem cell (PSC)-derived neurons have revealed the capacity of these neurons to self-organize into spontaneous active neuronal networks, generating concerted activities that are measured as synchronous bursting (Eiraku et al., 2008; Heikkilä et al., 2009; Illes et al., 2007, 2009). Therefore, PSC-neuronal networks display activities that in principle resemble those observed during brain function (Gullo et al., 2010a; Heikkilä et al., 2009; Illes et al., 2007, 2009; Nimmrich et al., 2005); however, the underlying mechanisms of the genesis of spontaneous activity and synchronicity have yet to be deciphered. This is crucial for understanding brain development and function, as well as for determining the proper use of PSC neurons in future transplantation approaches (Daadi et al., 2008; Eiraku et al., 2008; McDonald et al., 1999). Here, we hypothesize that IANs are responsible for the autonomous behavior of PSC-neuronal assemblies, i.e., spontaneous and synchronous neuronal network activities. Therefore,

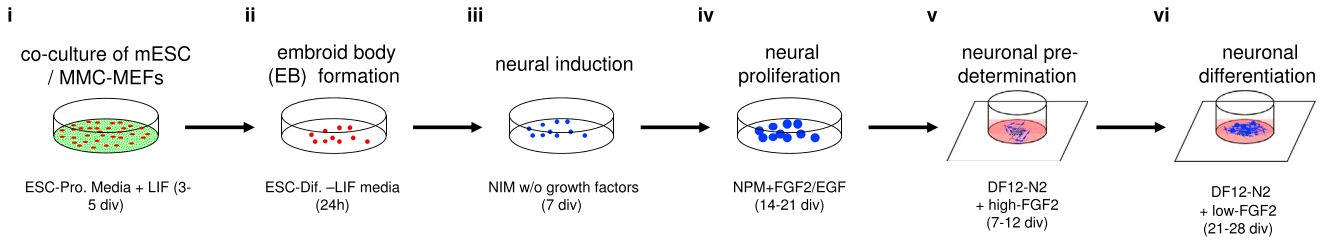

Figure 1. Generation of mESC-Derived Neuronal Networks

(i) mESCs were grown on mitomycin-inactivated mouse embryonic fibroblasts (MMC-MEFs) in the presence of leukemia inhibitory factor (LIF) for up to 5 days in vitro (5 div) followed by (ii) embryoid body (EB) formation in the absence of LIF. (iii) After 24 hr, free-floating EBs had developed and were replated in neural induction medium (NIM; for formulation, see Experimental Procedures). (iv) After 7 days, serum-free, floating cultures of EB-like aggregates (SFEB) had developed and were replated in NIM containing FGF2 and EGF. (v) After 14–21 div, nSFEBs were dissociated, stored in liquid nitrogen, or directly cultivated on PDL/laminin-coated MEAs in the presence of FGF2 in order to induce neuronal predetermination. (vi) FGF2 concentration was gradually decreased in the medium to induce terminal differentiation and neuronal network development. For a detailed description of neuronal composition and neuronal network development, see Illes et al. (2009).

we tested for the presence of neurons that became active after pharmacological inhibition of FSC, a cardinal feature of IANs, and determined whether these putative IANs were functionally integrated into the neuronal network. We further tested whether such FSC-independent neuronal activities relied on persistent sodium currents, another cardinal characteristic of IANs. Finally, we classified the putative IANs and discriminated between neurons that contributed to population bursts (PBs) and those that had pacemaker properties, based on a comparative analysis of network-wide PBs.

RESULTS

PSC-Neuronal Assemblies Show Robust Neuronal Activity in the Absence of FSC and Network Activity

We generated PSC neurons from murine embryonic stem cells (mESCs) by employing the widely-used *s*erum-free, *f*loating cultures of *e*mbryoid *b*ody-like aggregates (SFEB)-based protocol for neural differentiation of human and mouse PSCs (Eiraku et al., 2008; Gaspard et al., 2009; Heikkilä et al., 2009; Illes et al., 2009; Watanabe et al., 2005; Figure 1), which allows the generation of functional neuronal networks (Heikkilä et al., 2009; Illes et al., 2009). Dissociated mESC-derived neural cells were cultivated on MEAs and differentiated by gradual removal of growth factors from the medium (Figure 2). Weekly MEA recordings revealed that neuronal cells matured into neuronal networks starting with spontaneous activity 1 week after growth factor removal, and matured into either partly synchronously active (showing PBs) or unsynchronized active neuronal networks within 2–4 weeks (for details regarding the development of PSC-derived neuronal networks, see Heikkilä et al. [2009] and Illes et al. [2007]). In order to assess the presence of IANs in mature PSC-neuronal networks, both inhibitory and excitatory FSCs were consecutively blocked by pharmacological components (Figures 2A; Figure S1B available online; see Experimental Procedures) in mature neuronal networks. As described previously (Illes et al., 2007, 2009), PSC-neuronal networks show spontaneous asynchronous or partly synchronous activities (Figures 2B–2D, i) that are highly synchronously active after application of the $GABA_A$ receptor antagonist gabazine (Figures 2B–2D, ii, and S1B). Thus, PSC-neuronal assemblies harbor neurons that are functionally interconnected, but the occurrence of PBs is apparently inhibited by GABAergic neurons. The gabazine-induced disinhibition is characterized by high-frequency PBs (Figures 2B–2D, ii, and S1B) and high synchronicity (Figures 2Eiii, and S1B).

Other investigators and we have demonstrated that PSC-derived neural stem cells generate a large fraction of GABAergic neurons (~70% of all neuronal cells) as well as a substantial amount of glutamatergic neurons (Eiraku et al., 2008; Illes et al., 2009; Watanabe et al., 2005). Moreover, in PSC-neuronal networks, glutamatergic excitatory neurons contribute to spontaneous activity and mediate recurrent excitation, measured as high-frequency PBs under disinhibition conditions (Heikkilä et al., 2009; Illes et al., 2009). Here, we show that neither the neuronal activity nor the network coherences are influenced by glycine or acetylcholine treatment (Figure S5). Hence, PSC neurons develop into networks in which GABAergic inhibitory and glutamatergic excitatory neurons are persistently active in the absence of external input. To inhibit glutamatergic excitatory FSC in gabazine-treated PSC-neuronal networks, we added the NMDA-receptor

antagonist *D-AP-5* and then the AMPA/Kainate-receptor antagonist *NBQX* (hereafter abbreviated as G/A/N). Similar experiments using rat cortical and hippocampal neuronal cultures ensured the FSC blocking activities of G/A/N (Figures S2 and S3). Surprisingly, extracellular recordings of G/A/N-treated cultures demonstrated prominent residual neuronal activities (Figures 2B–2D, iii, and 2E), the absence of PBs (Figures 2B–2D, iii), and the lack of synchronous neuronal activity (Figure 2Eiii). Similar results were obtained after prolonged (60 min) application of G/A/N (Figure 2E), excluding the possibility that a short (15 min) treatment was insufficient to block FSC. Also, we tested the stability of primary cortical, hippocampal, and PSC-neuronal assembly systems, and were able to demonstrate the consistency of the network properties over at least 4 months, the latest time point that was systematically tested (Figures S2 and S3). Since extracellular calcium ions ($[Ca^{2+}]_e$) are required for synaptic neurotransmitter release, we performed MEA recordings of mESC-derived neuronal networks preincubated with artificial cerebrospinal fluid (aCSF) in the presence of the $GABA_A$-receptor antagonist gabazine and in the presence or absence of Ca^{2+} (Figure S1C). Although disinhibition in the presence of $[Ca^{2+}]_e$ transformed asynchronous active mESC-derived neurons into a highly synchronous active network, a few mESC-derived neurons remained active in the absence of $[Ca^{2+}]_e$ and did not show synchronous bursting under disinhibition conditions (Figure S1C). This demonstrates that in the absence of FSC mediated either by pharmacological compounds or by removal of $[Ca^{2+}]_e$, mESC-derived neurons remain active. Interestingly, 69% ± 38% of spike-detecting electrodes that were initially active in standard medium were still detecting neuronal activity in the absence of FSC, whereas only 10.6% ± 11.4% of spike-detecting electrodes that were initially active in aCSF were still detecting neuronal activity in the absence of FSC (compare Figures 2 and S2 with Figure S1). This demonstrates that in aCSF, fewer neurons are able to be active in the absence of FSC, which has been also reported for IANs of the spinal cord (Latham et al., 2000b).

In summary, the robust neuronal activities in PSC-neuronal networks recorded in aCSF and medium in the absence of inhibitory and excitatory FSC or $[Ca^{2+}]_e$ strongly suggest the presence of IANs in the system.

IANs Are Functionally Integrated into PSC-Neuronal Assemblies

Next, we analyzed whether IANs are functionally integrated into the neuronal network by characterizing the firing behavior of PSC neurons in the absence or presence of FSC. In comparison with standard medium and disinhibition conditions, the percentage of spikes that organized in bursts was strongly decreased in G/A/N-treated cultures (Figure 2Eii), whereas the average number of recorded spikes was only slightly reduced (Figure 2Ei). This suggests that in the absence of FSC, the majority of IANs fired in a spike mode instead of a bursting mode.

We used the number of spike-detecting electrodes as a rough estimate of the relative amount of neurons that were active in the presence and absence of FSC. Although the number of active electrodes was similar in standard medium compared with disinhibition conditions (24 ± 12 versus 25 ± 13 out of 60 electrodes, n = 18), it was significantly reduced in the absence of FSC (16 ± 6 out of 60 electrodes, n = 18; Figure 2Eiv). Since one electrode might simultaneously detect the spike activities of several neurons, we used spike-sorting analysis to discriminate among activities derived from multiple neurons. Given that each neuron tends to fire spikes of a particular morphology and kinetics (Quiroga, 2007), we grouped spikes into clusters based on the similarity of their shapes, amplitudes, and organizations, each of which was presumably generated by an individual IAN (Quiroga, 2007) (see Experimental Procedures; Figure 3). In the absence of FSC, the vast majority of electrodes recorded activity from either a single neuron (71 out of 94 active electrodes, ~76%) or two neurons (14 out of 94 active electrodes, ~15%). Occasionally, activity was associated with three (8 out of 94 active electrodes, ~8%) or four neurons (1 out of 94 active electrodes, ~1%; Figure S4). The initial spike shapes recorded at a specific electrode from individual IANs were maintained in the presence of FSC (Figure 3), demonstrating that IANs are still active in the presence of FSC. Therefore, 69% of the electrodes that were initially active under standard medium were still detecting neuronal activity with characteristic spike morphologies in the absence of FSC. This suggests that a substantial amount of the PSC neurons detected under standard conditions were IANs.

To confirm the functional integration of IANs at the cellular level, we used calcium imaging to validate that morphologically identified cells with ascending neurites showed spontaneous activity in the presence of FSC in whole-cell patch-clamp recordings (Figure 4Ai). Immunocytochemistry staining confirmed the synaptic integration of recorded neurons (Figure 4Aii). Combined MEA, calcium, and whole-cell patch-clamp recordings revealed that some neurons located in close proximity (within 50 μm) to a burst-detecting electrode showed prominent calcium waves synchronously with network-wide PBs (Figure 4B), and whole-cell patch-clamp recordings showed intrinsic activity in the absence of FSC (Figure 4C). Thus, in summary, IANs are functionally integrated into PSC-neuronal networks.

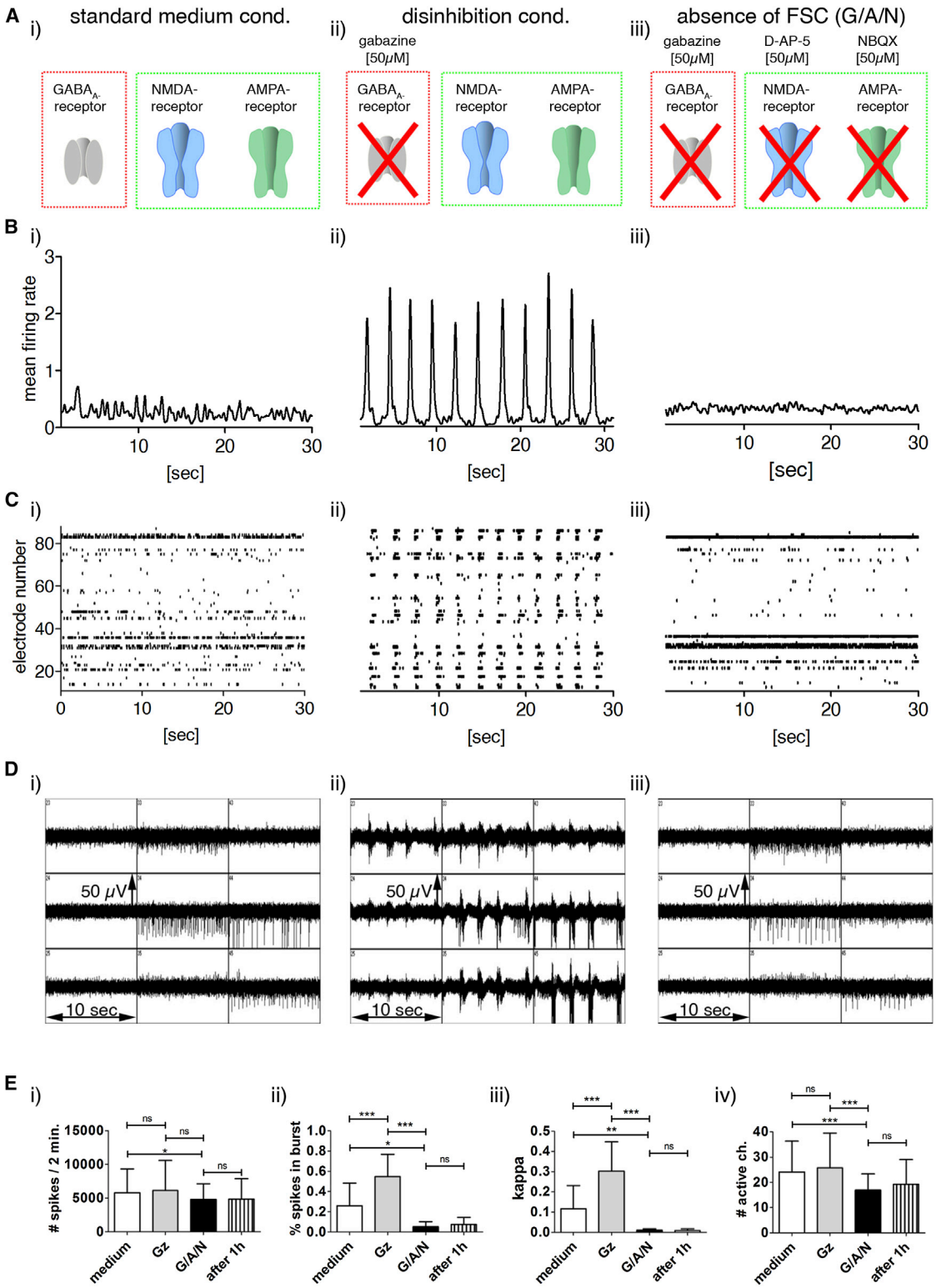

Figure 2. Activity of PSC Neurons in the Presence and Absence of FSC

(A) Drawings illustrate inhibitory (red box) and excitatory (green box) neurotransmitter receptors, and indicate the antagonists used.

(B) Mean firing rates (MFRs; 100 ms smoothed spike count in bin [spikes in 10 ms intervals]).

(legend continued on next page)

The Autonomous Activity of IANs Depends on Persistent Active Sodium Channels, but Not on L-Type Calcium Channels

We recently demonstrated that tetrodotoxin (TTX) application completely blocks neuronal activity in PSC-neuronal cultures (Illes et al., 2007), indicating that intrinsic neuronal activity depends on voltage-gated sodium channels. The autonomous activity of IANs in different brain regions has been shown to depend on persistent riluzole-sensitive sodium currents (Atherton and Bevan, 2005; Atherton et al., 2008; Beatty et al., 2012; Guzman et al., 2009; Tazerart et al., 2008; Yvon et al., 2007). Here, we demonstrated that riluzole completely blocked the IAN activity in G/A/N-treated PSC-neuronal assemblies (Figures 5A and 5B), indicating that the autonomous activity of IANs depends on persistent sodium currents.

The activity of IANs in certain brain regions, such as the striatum (Puopolo et al., 2007), is modulated by L-type voltage-gated calcium channels (LTCCs). Therefore, we determined whether autonomously active PSC IANs are regulated by LTCCs. We found that neither the spiking nor the bursting activities of autonomously active IANs were affected by the application of either the LTCC antagonist isradipine (4 μM) or the LTCC agonist FPL64176 (2 μM) for 15 or 60 min (Figures 5C–5E). Taken together, these results indicate that the autonomous activity of PSC IANs relies on persistent sodium currents, but not on LTCC activity.

IANs Have Diverse Intrinsic Firing Behaviors

Since different populations of IANs within the brain differ with respect to their intrinsic firing behaviors (Atherton and Bevan, 2005; Atherton et al., 2008; Beatty et al., 2012; Beurrier et al., 2000; Feldman and Del Negro, 2006; Forti et al., 2006; Le Bon-Jego and Yuste, 2007), we classified PSC-derived IANs according to their activity in the absence of FSC. We based the electrophysiological classification of IANs on the spike frequency, regularity, and organization (i.e., single events, trains of spikes, or bursts). In the absence of FSC, IANs displayed five different firing modes: (1) regular spiking characterized by constant interspike intervals (Figure 6A), (2) irregular spiking characterized by variable interspike intervals (Figure 6B), (3) stuttering characterized by the generation of trains of spikes (Figure 6C), (4) bursting (Figure 6D), and (5) mixed firing characterized by the generation of spikes and bursts (Figure 6E). Therefore, similarly to IANs in the brain (Atherton and Bevan, 2005; Atherton et al., 2008; Beatty et al., 2012; Beurrier et al., 2000; Feldman and Del Negro, 2006; Forti et al., 2006; Le Bon-Jego and Yuste, 2007; Mao et al., 2001; Tazerart et al., 2008), IANs in PSC-derived neuronal assemblies represent a heterogeneous group with distinct electrophysiological intrinsic firing behaviors.

The Firing Behavior of IANs Correlates with Network Activity and Shows Pacemaker-Like Properties

As described above, IANs are functionally integrated into neuronal assemblies and contribute to network-wide PBs. However, to discriminate between IANs that only contribute to PBs and those that have pacemaker properties, we analyzed the firing behavior of IANs during PBs in more detail. For this purpose, we used shape-based spike sorting of extracellular recorded spikes and compared the firing behaviors of individual IANs in the absence of FSC and under disinhibition conditions (Figure 3). Interestingly, the firing frequency and regularity of the IANs changed during PBs, indicating that all neurons with IANs properties are functionally integrated in PSC-neuronal assemblies.

PBs in disinhibited cultures started with synchronous temporal discharges of several spatially distributed neurons, indicated as peaks in the mean-firing diagram (phase I of PB; see Figures 7B and 7C), followed by a decrease in neuronal firing (phase II of PB; Figures 7B and 7C), and terminated by a refractory period in which neuronal activity was minimal and not synchronous until the next PB

(C) Spike raster plots (SRPs).
(D) Original traces of nine channels of an MEA recording.
(E) Diagrams showing neuronal activity in standard medium (i in B–D, white bars in E), disinhibition conditions (ii in B–D, gray bars in E), and after inhibition of GABAergic and glutamatergic FSC (iii in B–D, black bars in E) in PSC-neuronal networks.
(B) MFRs show the (ii) appearance or (i and iii) absence of PB.
(C) In SRPs, each dot represents a spike recorded by one electrode at a certain time point.
(D) In original traces of MEA recordings, each box shows a 10 s extracellular recording detected by one electrode.
(E) Diagrams show (i) the mean number (#) of extracellularly recorded spikes in 2 min, (ii) the percentage of spikes organized as bursts, (iii) the network synchrony indicated as Cohen's kappa, and (iv) the number of spike-detecting electrodes under standard medium conditions or disinhibition conditions (Gz, gabazine treatment), and after 15 min and 1 hr inhibition of FSC (G/A/N = gabazine, *D-AP-5*, and *NBQX* treatment). n = 17; data are mean values ± SD (t test; ns, not significant; *p < 0.05, **p < 0.01, ***p < 0.001. See also Figure S1 for the activity of mESC-derived IANs under aCSF. See Figure S2 for the activity of IANs in prolonged cultured PSC, primary cortical, and hippocampal neuronal assemblies, and Figure S3 for the activity of IANs 15 min and 60 min after the application of G/A/N.
See also Table S1 and S2.

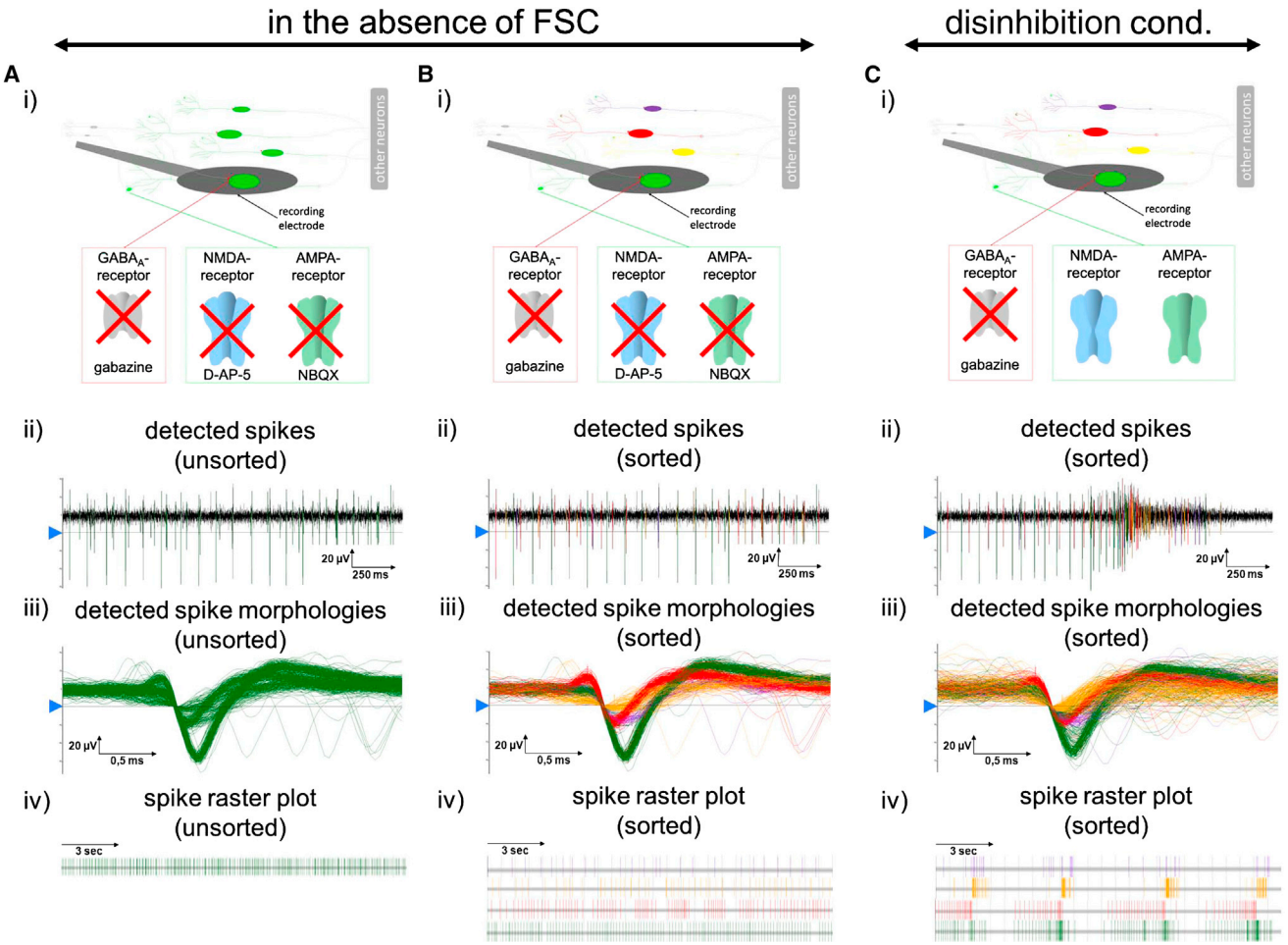

Figure 3. Identification of Individual IAN Activities by Spike Sorting

(A–C) (i) Schematic drawings illustrate four neurons in close proximity to one extracellular recording electrode. Unsorted (A) and sorted (B and C) spikes were recorded by one electrode (A and B) in the absence of FSC (G/A/N) and (C) under disinhibition conditions (Gz, gabazine treatment). Identified spike shapes are visualized as (ii) original traces, (iii) superimposed spikes (temporal resolution of 25 kHz), and (iv) SRPs. After manual determination of the detection level (blue arrow in ii and iii), distinct spikes were marked according to their spike shapes and visualized by different colors. See also Figure S4 for examples of recorded spike morphologies.
See also Table S2.

(phase III of PB; Figures 7B and 7C). IANs were classified into four types according to their firing behaviors during PB. Type I represents IANs that are completely inactive in disinhibited neuronal networks (Figure S6E), suggesting that the presence of FSC blocked neuronal activity in this IAN type. Type II IANs were specifically and exclusively active during PB, and not during the refractory period of PB (Figures 7A and 7B). In contrast, type III IANs were active during PB as well as during the refractory period of PB (Figures 7A and 7B). Finally, type IV IANs showed increasing neuronal activity during the refractory period of PB (phase III), culminating in a high-frequency burst prior to the onset of PB, and became inactive during PB. Concomitantly with the decline of PB (phase II of PB), type IV IANs gradually recovered activity (Figures 7B, 7C, and S6A–S6D). Thus, the reciprocal temporal pattern of the activity of type IV IANs and the appearance of PB in the neuronal network indicates that type IV neurons act as pacemaker neurons in the network.

DISCUSSION

Here, we have demonstrated the existence of IANs in PSC-neuronal networks. These neurons are active in the absence of FSC and depend on voltage-gated as well as persistent active sodium channels. They are functionally integrated into PSC-neuronal assemblies and contribute

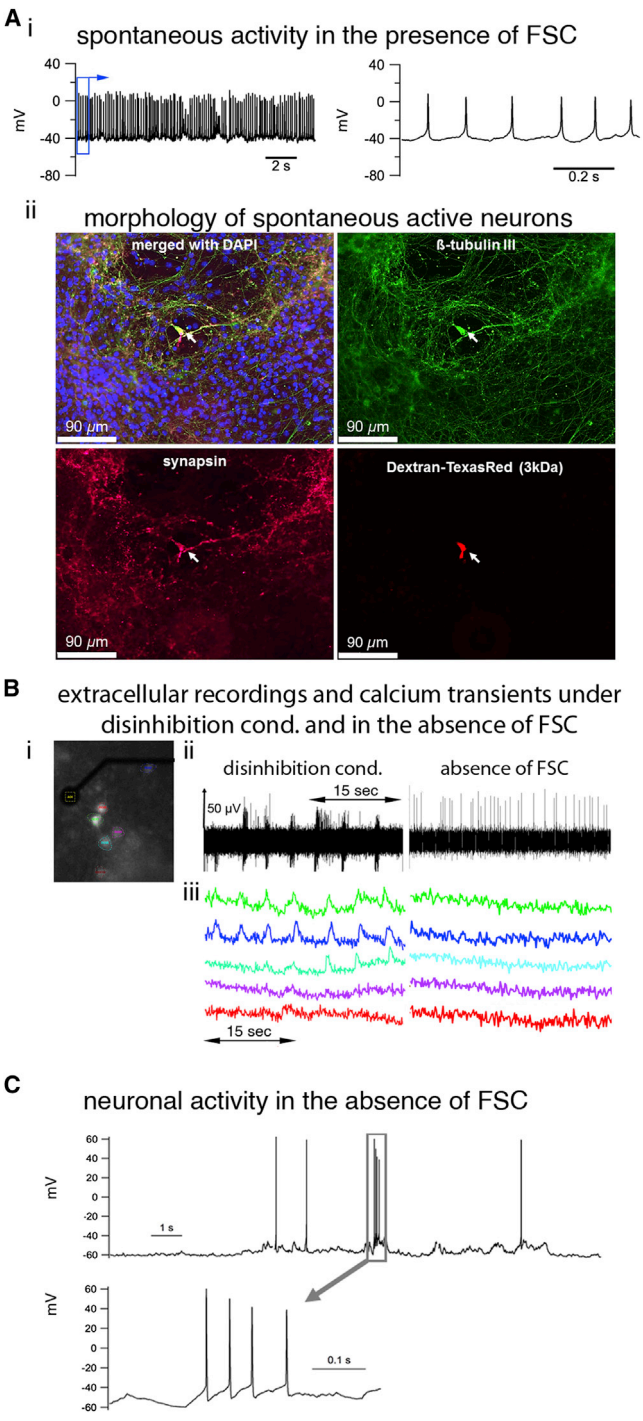

Figure 4. IANs Are Functionally Integrated into PSC-Neuronal Networks

(A) (i) Membrane potential recording of a neuron showing spontaneous action potential firing in the presence of FSC. The segment of the left trace framed by the blue rectangle is shown on the right with a different timescale. (ii) Dextran-Texas red-labeled neurons were ßtubulinIII$^+$ and possessed synaptophysin$^+$ synapses. The images show the neuron from which the recording in (i) was obtained.

(B and C) Simultaneous MEA recordings and calcium imaging under disinhibition conditions and in the absence of FSC (B), followed by whole-cell patch clamp recording in the absence of FSC (C).

(B) (i) Calcium imaging of PSC neurons cultivated on MEAs for 28 days, preincubated with the calcium indicator Fluo-4/AM, and treated with gabazine (50 µM; disinhibition condition) or with AP-5 (30 µM), NBQX (30 µM each), and gabazine (50 µM; absence of FSC). Colored regions (ROIs) indicate cells that are in close vicinity to the recording electrode. (ii) Simultaneous extracellular recorded PB and (iii) calcium transients in Fluo-4/AM-loaded PSC neurons (y axis: relative fluorescence units [RFU]). Calcium traces in (iii) correspond to ROIs in (i).

(C) Representative trace of a membrane potential recording of a single neuron shows irregular action potential firing and bursting in the absence of FSC. The lower tracing is an expanded view of the action potential burst framed in the upper tracing by a gray rectangle.

See also Table S2.

to network activities. IANs represent a heterogeneous group of neurons that are characterized by their specific contributions to PBs. Moreover, a specific subtype of IANs (type IV) exhibits a firing behavior that is typical of pacemaker neurons, i.e., firing reciprocally to synchronous network activity.

Most Spontaneously Active PSC Neurons Are IANs

PSC-neuronal cultures consist of (1) nonspontaneously active neurons, in which action potentials can be induced by electrical stimulations (Risner-Janiczek et al., 2011); (2) spontaneously active neurons, which become active without electrical stimulation (Heikkilä et al., 2009; Illes et al., 2007, 2009); or (3) silenced neurons, in which activity is suppressed through GABAergic inhibitory synapses (Illes et al., 2009). Here, we found that only 40% ± 20% of the electrodes (24 ± 12 out of 60, n = 18 standard medium) recorded spontaneous activity, and that Fluo-4/AM-loaded PSC neurons located close to recording electrodes showed neither calcium waves nor neuronal activities even under disinhibition conditions. This absence of activity indicates that several electrodes were covered by neurons that were not spontaneously active. These extracellular recordings confirm a previous patch-clamp analysis of PSC neurons (Risner-Janiczek et al., 2011) and demonstrate that the minority of PSC neurons are spontaneously active in the presence of FSC. Interestingly, electrophysiological analyses of PSC neurons suggested that spontaneous activity of PSC neurons is induced solely by synaptic communication (Eiraku et al., 2008; Espuny-Camacho et al., 2013; Weick et al., 2011). However, by comparing the number of spike-detecting electrodes in the presence and absence of FSC, we showed that 69% of spike-detecting electrodes that were initially active under standard medium were still detecting neuronal activity in the absence

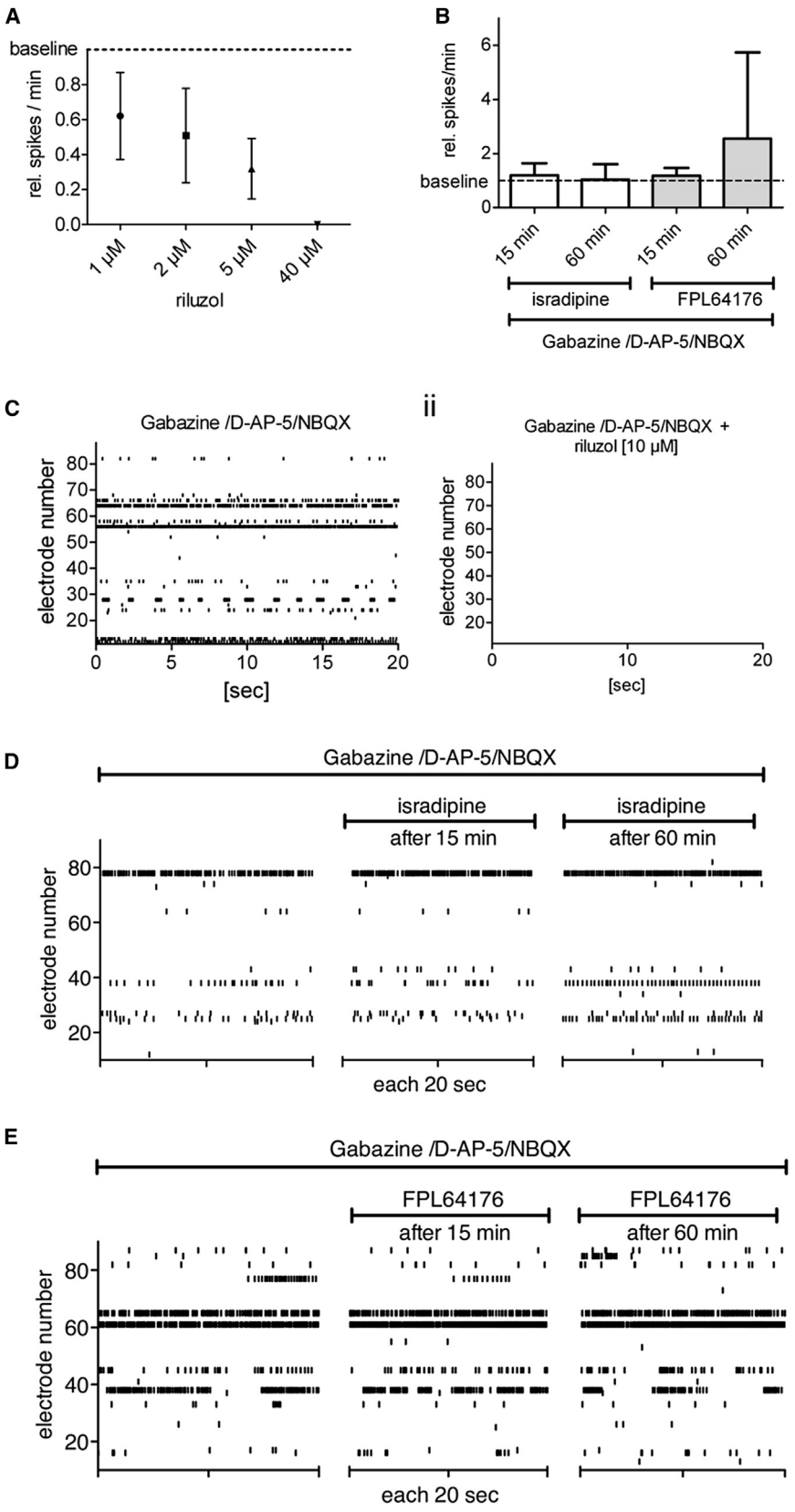

Figure 5. The Autonomous Activity of IANs Depends on Persistent Active Sodium Channels, but Not on LTCCs

(A–E) PSC neurons cultivated on MEAs were preincubated with G/A/N and treated with (A and C) the persistent sodium current blocker riluzole or (B, D, and E) the LTCC antagonist isradipine or LTCC agonist FPL64176.

(A) Concentration-dependent impact of riluzole on neuronal activity (n = 5).

(B) Impact of isradipine and FPL64176 on neuronal activity after 15 min and 60 min (n = 5 each).

(C) Representative SRPs (i) before and (ii) after the application of 10 µM riluzole.

(D and E) Representative SRPs before and after the application of (D) isradipine and (E) FPL64176. Data are mean values ± SD. See also Figure S5 for the impact of acetylcholine and glycine on the spontaneous neuronal activity of PSC neurons. See also Table S1 and S2.

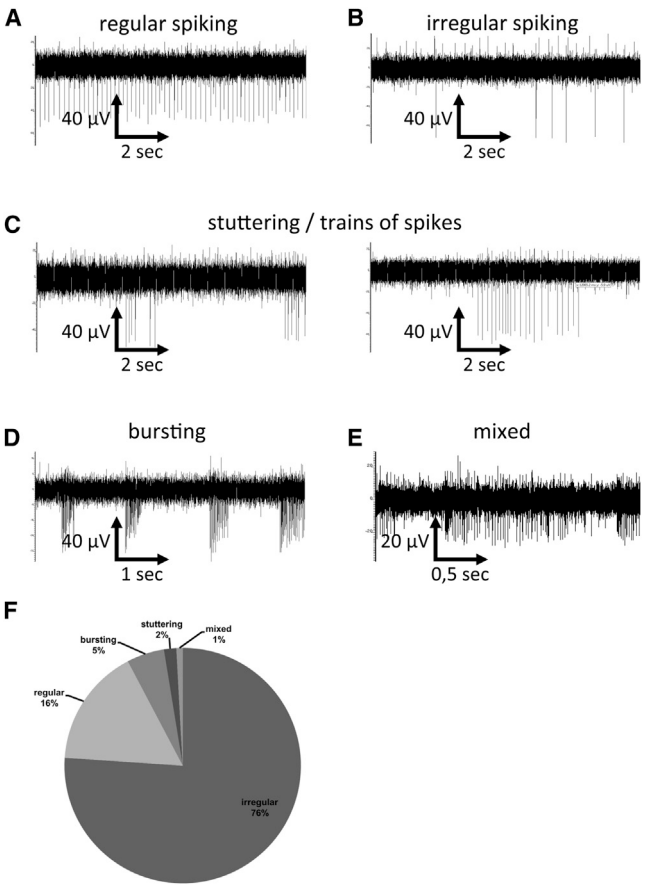

Figure 6. Firing Behavior of IANs in the Absence of FSC

(A–E) Representative recordings of extracellular signals in PSC-derived neuronal assemblies treated with G/A/N. Five different firing modes of IANs are shown: (A, i) regular spiking, (B) irregular spiking, (C) stuttering, (D) bursting, and (E) mixed firing (spiking and bursting) activity.

(F) Quantification of the different firing behaviors of IANs in the absence of FSC (n = 124).

See also Table S2.

of FSC. In addition, we showed that this synaptic-communication-independent activity disappeared after the blocking of persistent sodium currents. Therefore, the spontaneous activity of PSC neurons is not induced solely by synaptic communication, but also depends on intrinsic mechanisms. Considering the present findings, it is astonishing that IANs have remained unnoticed for so long in PSC neuronal cultures. One explanation for this might lie in the experimental details. For example, previous electrophysiological analyses of mouse and human PSC-derived neurons were performed in aCSF. Here, we demonstrated that only a few IANs were autonomously active in conditions using aCSF, and therefore these activities might simply have been overlooked in the past. In addition, standard low-temporal-resolution calcium imaging is not applicable to visualize calcium transients in IANs (Figure 4B, absence of FSC) (Eiraku et al., 2008). For example, although calcium imaging systems with a temporal resolution of >3 ms were useful for the visualization and identification of calcium transients in bursting neurons (Figure 3; Eiraku et al., 2008), they were inappropriate for the detection of spike-associated calcium transients generated by IANs (Figure 4B, absence of FSC). Nevertheless, we showed that a combined setup of calcium imaging and whole-cell patch-clamp recordings under medium conditions was able to provide intracellular recordings of the autonomous activity of IANs. Thus, we confirm that PSC-neuronal populations consist of inactive, silenced, and spontaneously active neurons (Illes et al., 2007, 2009; Risner-Janiczek et al., 2011), and demonstrated that most of these spontaneously active neurons are IANs, having the ability to be active in the absence of synaptic input.

Mechanisms of Autonomous Activity in IANs

Similar to what was previously observed for IANs in brain slices (Atherton and Bevan, 2005; Atherton et al., 2008; Beatty et al., 2012; Guzman et al., 2009; Tazerart et al., 2008; Yvon et al., 2007), we found that the intrinsic activity of PSC IANs depended on voltage-gated sodium channels and persistent sodium currents (Illes et al., 2007). However, and in contrast to pacemaker neurons of different brain regions (Atherton et al., 2008; Darbon et al., 2002a; Guzman et al., 2009), the intrinsic activity of PSC IANs did not depend on LTCCs. Moreover, we excluded other synaptic systems, such as glycinergic and acetylcholinergic neurotransmission, from being involved in the intrinsic activity of PSC neurons. Therefore, we demonstrated that the autonomous activity of IANs within PSC-neuronal assemblies was not mediated by synaptic communication, but rather depended on intrinsic mechanisms such as persistently active sodium channels. At present, the possibility that other ion channels or neurosteroids (Puia et al., 2012) contribute to or influence autonomous activity in IANs cannot be excluded and will be the subject of future investigations.

Function of IANs

The probability that a PB will appear within a neuronal assembly depends on the connectivity of the neurons (Arnold et al., 2005; Ivenshitz and Segal, 2010; Latham et al., 2000a), the interplay of excitatory and inhibitory neurotransmitter systems (Brunel and Wang, 2003), and the proportions and properties of the IANs within a neuronal network (Bazhenov et al., 2008; Latham et al., 2000a, 2000b). Experimental data and mathematical models have indicated that neuronal assemblies with a relatively high proportion of active IANs show fewer

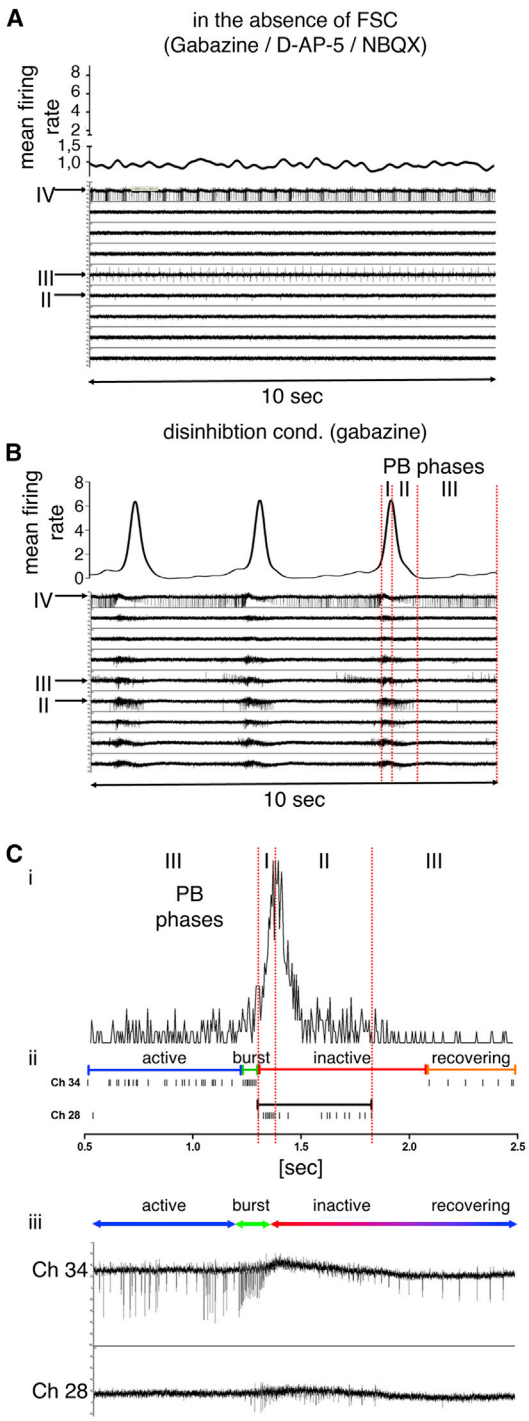

Figure 7. Firing Behavior of IANs in the Presence of FSC and Network Activity

(A–C) Firing behavior of IANs and non-IANs in the absence (A) or presence (B–C) of network activity. Upper traces in A–C: MFR, 100 ms smoothed spike count in bin (spikes in 5 ms intervals)) indicating the absence or appearance of PB (indicated as peaks). Roman numerals indicate the different phases of PB. Lower traces in A and B: MEA recordings showing the firing behavior of type II, III, and IV IANs (indicated by arrows), and five non-IANs in the absence or presence of PB.

(C) A detailed example of the firing behavior of type IV IANs during PBs is depicted. (i) MFR (unsmoothed spike count in bin [spikes in 5 ms]) indicates the appearance of PBs, (ii) SRP, and (iii) electrode raw data of type IV IANs (channel 34) and non-IANs (channel 28). Colored lines correspond to the four phases of the firing behavior of type IV IANs.

See also Figure S6 for the morphologies of spikes generated from type IV IANs, and for the firing behavior of type I IANs. See Figure S7 for the firing characteristics of mESC-derived IANs during PBs.

See also Table S2.

spontaneous PBs (Latham et al., 2000a, 2000b). Indeed, our experimental results clearly show that, although highly synchronously active cortical and hippocampal neuronal cultures contained few IANs, asynchronously active PSC-neuronal assemblies contained a large number of IANs. Moreover, we demonstrated that under aCSF conditions, mESC-neuronal networks became synchronously active, and only a few IANs were able to be autonomously active under such conditions. In accordance with other experimental data and theoretical models (Latham et al., 2000a, 2000b), we assume that reducing the number of active IANs by aCSF leads to an increased probability of PBs occurring. Therefore, the number of active IANs within neuronal networks is a critical parameter for assessing the probability of the occurrence of distinct network activity stages, such as PB.

The IANs described herein have four different firing behaviors. Type I IANs are completely inactive in disinhibited networks. Most likely, synaptic input might completely "overrule" intrinsic neuronal activity, and this silencing might exclude specific IANs from neuronal network activity under defined activity states. In contrast, type II and type III IANs are active during PB, suggesting that these IANs are recruited by neuronal cell populations to contribute to neuronal processing. In a recent study, a combination of MEA recording with fluorescence imaging of neocortical cultures from mice expressing GFP in GABAergic cells revealed that bursts of GABAergic neurons during PB are characterized by a burst duration of >250 ms and comprise more than ten spikes per burst (Becchetti et al., 2012), whereas excitatory neurons show a shorter burst duration and fewer spikes per burst (Becchetti et al., 2012; Pouille and Scanziani, 2001). Therefore, we compared the burst characteristics of type II and III IANs during synchronous PBs (Figure S7). The synchronous bursting of type II and III is characterized by a burst duration of 240–1,010 ms (mean ± SD = 486 ± 196, n = 37; Figure S7) and number of spikes per burst of 7.3–27.6 (mean ± SD = 13.6 ± 4.8, n = 37; Figure S7). Since other investigators

and we have demonstrated that ~70% of mESC-derived neurons generated by the default SFEB protocol are GABAergic (Eiraku et al., 2008; Illes et al., 2009; Watanabe et al., 2005), and the burst characteristics presented here indicate a GABAergic rather than a excitatory identity, we conclude that type II and III IANs are GABAergic.

Since the appearance of PBs within the network requires intrinsic triggers, type III IANs, which are capable of being spontaneously active before PBs, might be involved in modulating the appearance of PBs. In contrast to type I, II, and III IANs, type IV IANs represent a minor population in PSC-neuronal assemblies and have a unique firing behavior that is reciprocal to synchronous PBs. Similar firing behaviors have been reported for HUB neurons localized within the CA3 region of the hippocampus (Bonifazi et al., 2009), neurons within the CA1 pyramidal layer of the hippocampus (Fuentealba et al., 2008), pacemaker neurons localized within the central pattern generator (CPG) of the spinal cord (Darbon et al., 2002b), and CV1a neurons within the feeding CPG in the buccal ganglia (Harris et al., 2010). Based on our observations, we assume that type IV IANs act as pacemaker neurons that induce synchronous bursting in disinhibited PSC-neuronal assemblies. Type IV IANs have a burst duration of <250 ms, similar to what has been observed for excitatory neurons (Becchetti et al., 2012). However, the number of spikes per burst being $\geq$8 is more typical of inhibitory neurons (Becchetti et al., 2012; Figure S6). Therefore, the inhibitory or excitatory identity of type IV IANs remains a subject for future investigations.

EXPERIMENTAL PROCEDURES

Generation of mESC-Derived Neural Cells

ESC lines SV-129 and C57Bl6 (ATCC; Millipore) were differentiated into a neuronal lineage according to previously published protocols (Illes et al., 2009); for details, see the Supplemental Experimental Procedures. For an overview of the cell lines that were used for individual experiments, see Table S2. For a detailed description of the neuronal composition, see Illes et al. (2009) and Watanabe et al. (2005).

Analyses of MEA Recordings in PSC, Cortical, and Hippocampal Neuronal Networks

To measure the electrophysiological activity of mESC-derived neuronal networks, frozen stocks of dissociated neural precursor cell-enriched SFEB (nSFEB) cells were thawed and 60,000 cells were cultivated on poly-D-lysine (PDL)/laminin-coated MEAs for up to 4 months as described previously (Illes et al., 2009). Primary cortical and hippocampal neurons were obtained from isolated embryonic cortex or hippocampal tissue, respectively, and cultivated on MEAs according to published protocols (Arnold et al., 2005). Detailed descriptions of the neuronal composition of primary cortical and hippocampal neuronal cultures can be found elsewhere (Benson et al., 1994; Cáceres et al., 1986; de Lima et al., 2007, 2009; Gullo et al., 2010b; Sahara et al., 2012). Neuronal activity was recorded on a weekly basis to monitor neuronal network development. Only mature neuronal networks in culture for more than 3 weeks were analyzed. As described elsewhere (Illes et al., 2009), the MEAs used had a square grid of 60 planar Ti/TiN electrodes (30 μm diameter, 200 μm spacing) and an input impedance of <50 kOhm according to the specifications of the manufacturer (Multi Channel Systems). Signals from all 60 electrodes were simultaneously sampled at 25 kHz, visualized, and stored using the standard software MC_Rack provided by Multi Channel Systems. Spike and burst detection was performed offline with custom-built software (Result GmbH) as described elsewhere (Illes et al., 2009).

Statistics

Data are presented as means ± SDs; n refers to the number of independent recordings in independent neuronal assemblies. The statistical significance of differences between groups was determined using the paired t test (GraphPadPrism, version 5.0); p values below 0.05 were considered significant; p values of <0.05, 0.01, and 0.001 are indicated as *, **, and ***, respectively. Individual p values for the different experiments are given in Table S1.

Cell Membrane Potential and Intracellular Ca^{2+} Recordings

mESC-derived neurons were cultured in neural differentiation medium on PDL-laminin-coated glass coverslips (1 cm diameter) or MEAs and used for patch-clamp or Ca^{2+} imaging after 3 weeks in culture, respectively. The coverslips were transferred to a recording chamber (Warner Instruments) and mounted on a Nikon TE2000-U inverted microscope. For combination with MEA recordings, the MEA system was mounted on the inverted microscope. Experiments were performed at room temperature in standard cell culture medium. Gabazine, *D-AP-5*, and *NBQX* (end concentration: 50 μM each) were added to this extracellular solution.

For measurements of intracellular Ca^{2+}, cells were loaded with Fluo-4/AM for 30 min at 37°C, followed by 30 min at room temperature. The light source was equipped with a mercury short arc lamp and an integrated shutter (LEJ Leistungselektronik Jena), and coupled to the microscope (Nikon TE2000-U) via a liquid light guide. The light was passed through a filter cube comprising a 340–380 nm excitation filter, a 440 nm dichroic mirror, and a 435–485 nm emission filter. Then 16-bit grayscale images with a binning of 1 × 1 were captured every 5 s (exposure time ranged from 100 to 400 ms) with a cooled CCD camera (SensiCam; pco). The camera and shutter were controlled by TILLvisION software, which was also used for analysis. Neurons with bright calcium signal defined the regions of interest (ROIs). Neurons were identified according to their round soma showing neurites, and the neuronal identity of these cells was further confirmed by intracellular recordings and immunocytochemistry (Figure 4). ROI signals were calculated by subtracting background noise from measured signal.

Membrane potential recordings were performed in the whole-cell patch-clamp configuration in the zero-current clamp mode.

Patch electrode resistances were 3–5 MΩ. Data were acquired and analyzed using an EPC-10 amplifier and PatchMaster/FitMaster software (HEKA). The pipette solution consisted of (in mM) 125 K-gluconate, 4 KCl, 2 $MgCl_2$, 10 HEPES free acid, 10 EGTA, 43 mannitol, 4 Mg-ATP. The pH was titrated to 7.3 with KOH 296 mOsm/kg as measured with a vapor pressure osmometer (Wescor). Experiments were performed at room temperature in standard cell culture medium.

Labeling and Immunocytochemistry of Intracellular Recorded Neurons

Loading of the cells with pipette solution containing 0.1 mg/ml 3 kDA Dextran-Texas red (Molecular Probes) was accomplished by passive diffusion from the recording electrode during electrophysiological data collection and for an additional 15 min thereafter. The cells were then washed in PBS and fixed for 15 min in 4% paraformaldehyde before incubation with 1% normal goat serum (NGS; Sigma) in PBS for 1 hr. The primary antibodies were monoclonal mouse antibodies to βtubulin III (1:750; R&D Systems) and were applied at 4°C overnight. After the cells were washed in PBS, the appropriate secondary antibodies coupled to Cy2 (Dianova) were applied for 1 hr at room temperature. The cells were counterstained for 1 min with DAPI (2 g/ml; Serva) to visualize cell nuclei.

Pharmacological Treatment

MEA experiments were performed at 37°C in standard cell culture medium or aCSF. Gabazine, D-AP-5, and NBQX (end concentration: 50 μM each) were consecutively added to this extracellular solution. Riluzole (1, 2, 5, or 40 μM), isradipine (4 μM), or FPL 64176 (2 μM; all from Tocris Bioscience) were applied after the inhibition of excitatory and inhibitory FSC. Dose responses were analyzed by consecutively increasing the concentration of AP-5, NBQX, or riluzole with 2 min of MEA recording and 5 min incubation time after application.

Spike Sorting

Spike sorting was performed by visual inspection and classification according the spikes' shape, amplitude, and appearance as single spikes or bursts (see Figures 3 and S4).

SUPPLEMENTAL INFORMATION

Supplemental Information includes Supplemental Experimental Procedures, seven figures, and two tables and can be found with this article online at http://dx.doi.org/10.1016/j.stemcr.2014.01.006.

ACKNOWLEDGMENTS

We thank J. Jadasz for invaluable comments and advice on this work, J. Gstöttner and M. Hertel for excellent technical assistance, and G. Bock (Institute of Pharmacy, Pharmacology and Toxicology, and Center of Molecular Biosciences, Innsbruck, Austria) for providing isradipine and FPL64176. This work was supported by the Austrian Science Fund, Special Research Funding Program SFB F4413-B19; Paracelsus Medical University (PMU-RISE R-11/04/028-Ill); the Research Commission of the Medical Faculty of Heinrich-Heine University Düsseldorf (FOKO 40/09); the European Union's Seventh Framework Programme (FP7/2007-2013) under grants HEALTH-F2-2011-278850 (INMiND) and HEALTH-F2-2011-279288 (IDEA); the Bavarian Elite Network; the Bavarian State Ministry of Sciences, Research and Arts (ForNeuroCell2); the German Federal Ministry of Education and Research (BMBF 01GN0978); the State Government of Salzburg (Austria); the Propter Homines Foundation; and the FWF Special Research Program (SFB) F44 "Cell Signaling in Chronic CNS Disorders."

Received: May 23, 2013
Revised: January 8, 2014
Accepted: January 16, 2014
Published: February 20, 2014

REFERENCES

Arnold, F.J., Hofmann, F., Bengtson, C.P., Wittmann, M., Vanhoutte, P., and Bading, H. (2005). Microelectrode array recordings of cultured hippocampal networks reveal a simple model for transcription and protein synthesis-dependent plasticity. J. Physiol. *564*, 3–19.

Atherton, J.F., and Bevan, M.D. (2005). Ionic mechanisms underlying autonomous action potential generation in the somata and dendrites of GABAergic substantia nigra pars reticulata neurons in vitro. J. Neurosci. *25*, 8272–8281.

Atherton, J.F., Wokosin, D.L., Ramanathan, S., and Bevan, M.D. (2008). Autonomous initiation and propagation of action potentials in neurons of the subthalamic nucleus. J. Physiol. *586*, 5679–5700.

Bazhenov, M., Timofeev, I., Fröhlich, F., and Sejnowski, T.J. (2008). Cellular and network mechanisms of electrographic seizures. Drug Discov. Today Dis. Models *5*, 45–57.

Beatty, J.A., Sullivan, M.A., Morikawa, H., and Wilson, C.J. (2012). Complex autonomous firing patterns of striatal low-threshold spike interneurons. J. Neurophysiol. *108*, 771–781.

Becchetti, A., Gullo, F., Bruno, G., Dossi, E., Lecchi, M., and Wanke, E. (2012). Exact distinction of excitatory and inhibitory neurons in neural networks: a study with GFP-GAD67 neurons optically and electrophysiologically recognized on multielectrode arrays. Front. Neural Circuits *6*, 63.

Benson, D.L., Watkins, F.H., Steward, O., and Banker, G. (1994). Characterization of GABAergic neurons in hippocampal cell cultures. J. Neurocytol. *23*, 279–295.

Beurrier, C., Bioulac, B., and Hammond, C. (2000). Slowly inactivating sodium current (I(NaP)) underlies single-spike activity in rat subthalamic neurons. J. Neurophysiol. *83*, 1951–1957.

Blankenship, A.G., and Feller, M.B. (2010). Mechanisms underlying spontaneous patterned activity in developing neural circuits. Nat. Rev. Neurosci. *11*, 18–29.

Bonifazi, P., Goldin, M., Picardo, M.A., Jorquera, I., Cattani, A., Bianconi, G., Represa, A., Ben-Ari, Y., and Cossart, R. (2009). GABAergic hub neurons orchestrate synchrony in developing hippocampal networks. Science *326*, 1419–1424.

Brunel, N., and Wang, X.J. (2003). What determines the frequency of fast network oscillations with irregular neural discharges? I. Synaptic dynamics and excitation-inhibition balance. J. Neurophysiol. *90*, 415–430.

Cáceres, A., Banker, G.A., and Binder, L. (1986). Immunocytochemical localization of tubulin and microtubule-associated protein 2 during the development of hippocampal neurons in culture. J. Neurosci. *6*, 714–722.

Daadi, M.M., Maag, A.L., and Steinberg, G.K. (2008). Adherent self-renewable human embryonic stem cell-derived neural stem cell line: functional engraftment in experimental stroke model. PLoS One *3*, e1644.

Darbon, P., Pignier, C., Niggli, E., and Streit, J. (2002a). Involvement of calcium in rhythmic activity induced by disinhibition in cultured spinal cord networks. J. Neurophysiol. *88*, 1461–1468.

Darbon, P., Scicluna, L., Tscherter, A., and Streit, J. (2002b). Mechanisms controlling bursting activity induced by disinhibition in spinal cord networks. Eur. J. Neurosci. *15*, 671–683.

de Lima, A.D., Lima, B.D., and Voigt, T. (2007). Earliest spontaneous activity differentially regulates neocortical GABAergic interneuron subpopulations. Eur. J. Neurosci. *25*, 1–16.

de Lima, A.D., Gieseler, A., and Voigt, T. (2009). Relationship between GABAergic interneurons migration and early neocortical network activity. Dev. Neurobiol. *69*, 105–123.

de Pasquale, F., Della Penna, S., Snyder, A.Z., Lewis, C., Mantini, D., Marzetti, L., Belardinelli, P., Ciancetta, L., Pizzella, V., Romani, G.L., and Corbetta, M. (2010). Temporal dynamics of spontaneous MEG activity in brain networks. Proc. Natl. Acad. Sci. USA *107*, 6040–6045.

Eiraku, M., Watanabe, K., Matsuo-Takasaki, M., Kawada, M., Yonemura, S., Matsumura, M., Wataya, T., Nishiyama, A., Muguruma, K., and Sasai, Y. (2008). Self-organized formation of polarized cortical tissues from ESCs and its active manipulation by extrinsic signals. Cell Stem Cell *3*, 519–532.

Espuny-Camacho, I., Michelsen, K.A., Gall, D., Linaro, D., Hasche, A., Bonnefont, J., Bali, C., Orduz, D., Bilheu, A., Herpoel, A., et al. (2013). Pyramidal neurons derived from human pluripotent stem cells integrate efficiently into mouse brain circuits in vivo. Neuron *77*, 440–456.

Feldman, J.L., and Del Negro, C.A. (2006). Looking for inspiration: new perspectives on respiratory rhythm. Nat. Rev. Neurosci. *7*, 232–242.

Forti, L., Cesana, E., Mapelli, J., and D'Angelo, E. (2006). Ionic mechanisms of autorhythmic firing in rat cerebellar Golgi cells. J. Physiol. *574*, 711–729.

Fuentealba, P., Tomioka, R., Dalezios, Y., Márton, L.F., Studer, M., Rockland, K., Klausberger, T., and Somogyi, P. (2008). Rhythmically active enkephalin-expressing GABAergic cells in the CA1 area of the hippocampus project to the subiculum and preferentially innervate interneurons. J. Neurosci. *28*, 10017–10022.

Gaspard, N., Gaillard, A., and Vanderhaeghen, P. (2009). Making cortex in a dish: in vitro corticopoiesis from embryonic stem cells. Cell Cycle *8*, 2491–2496.

Gullo, F., Maffezzoli, A., Dossi, E., and Wanke, E. (2010a). Identification of local field potentials and spikes on MEA256 platforms. Proceedings of the 7th International Meeting on Substrate-Integrated Micro Electrode Arrays.

Gullo, F., Mazzetti, S., Maffezzoli, A., Dossi, E., Lecchi, M., Amadeo, A., Krajewski, J., and Wanke, E. (2010b). Orchestration of "presto" and "largo" synchrony in up-down activity of cortical networks. Front. Neural Circuits *4*, 11.

Guzman, J.N., Sánchez-Padilla, J., Chan, C.S., and Surmeier, D.J. (2009). Robust pacemaking in substantia nigra dopaminergic neurons. J. Neurosci. *29*, 11011–11019.

Harris, C.A., Passaro, P.A., Kemenes, I., Kemenes, G., and O'Shea, M. (2010). Sensory driven multi-neuronal activity and associative learning monitored in an intact CNS on a multielectrode array. J. Neurosci. Methods *186*, 171–178.

Heikkilä, T.J., Ylä-Outinen, L., Tanskanen, J.M., Lappalainen, R.S., Skottman, H., Suuronen, R., Mikkonen, J.E., Hyttinen, J.A., and Narkilahti, S. (2009). Human embryonic stem cell-derived neuronal cells form spontaneously active neuronal networks in vitro. Exp. Neurol. *218*, 109–116.

Illes, S., Fleischer, W., Siebler, M., Hartung, H.P., and Dihné, M. (2007). Development and pharmacological modulation of embryonic stem cell-derived neuronal network activity. Exp. Neurol. *207*, 171–176.

Illes, S., Theiss, S., Hartung, H.P., Siebler, M., and Dihné, M. (2009). Niche-dependent development of functional neuronal networks from embryonic stem cell-derived neural populations. BMC Neurosci. *10*, 93.

Ivenshitz, M., and Segal, M. (2010). Neuronal density determines network connectivity and spontaneous activity in cultured hippocampus. J. Neurophysiol. *104*, 1052–1060.

Latham, P.E., Richmond, B.J., Nelson, P.G., and Nirenberg, S. (2000a). Intrinsic dynamics in neuronal networks. I. Theory. J. Neurophysiol. *83*, 808–827.

Latham, P.E., Richmond, B.J., Nirenberg, S., and Nelson, P.G. (2000b). Intrinsic dynamics in neuronal networks. II. experiment. J. Neurophysiol. *83*, 828–835.

Le Bon-Jego, M., and Yuste, R. (2007). Persistently active, pacemaker-like neurons in neocortex. Front. Neurosci *1*, 123–129.

Liu, Z., Fukunaga, M., de Zwart, J.A., and Duyn, J.H. (2010). Large-scale spontaneous fluctuations and correlations in brain electrical activity observed with magnetoencephalography. Neuroimage *51*, 102–111.

Mao, B.Q., Hamzei-Sichani, F., Aronov, D., Froemke, R.C., and Yuste, R. (2001). Dynamics of spontaneous activity in neocortical slices. Neuron *32*, 883–898.

McDonald, J.W., Liu, X.Z., Qu, Y., Liu, S., Mickey, S.K., Turetsky, D., Gottlieb, D.I., and Choi, D.W. (1999). Transplanted embryonic stem cells survive, differentiate and promote recovery in injured rat spinal cord. Nat. Med. *5*, 1410–1412.

Nimmrich, V., Maier, N., Schmitz, D., and Draguhn, A. (2005). Induced sharp wave-ripple complexes in the absence of synaptic inhibition in mouse hippocampal slices. J. Physiol. *563*, 663–670.

Pouille, F., and Scanziani, M. (2001). Enforcement of temporal fidelity in pyramidal cells by somatic feed-forward inhibition. Science *293*, 1159–1163.

Puia, G., Gullo, F., Dossi, E., Lecchi, M., and Wanke, E. (2012). Novel modulatory effects of neurosteroids and benzodiazepines on excitatory and inhibitory neurons excitability: a multi-electrode array recording study. Front. Neural Circuits *6*, 94.

Puopolo, M., Raviola, E., and Bean, B.P. (2007). Roles of subthreshold calcium current and sodium current in spontaneous firing of mouse midbrain dopamine neurons. J. Neurosci. *27*, 645–656.

Quiroga, R.Q. (2007). Spike sorting. Scholarpedia *2*, 3583.

Risner-Janiczek, J.R., Ungless, M.A., and Li, M. (2011). Electrophysiological properties of embryonic stem cell-derived neurons. PLoS ONE *6*, e24169.

Sahara, S., Yanagawa, Y., O'Leary, D.D., and Stevens, C.F. (2012). The fraction of cortical GABAergic neurons is constant from near the start of cortical neurogenesis to adulthood. J. Neurosci. *32*, 4755–4761.

Shew, W.L., Bellay, T., and Plenz, D. (2010). Simultaneous multielectrode array recording and two-photon calcium imaging of neural activity. J. Neurosci. Methods *192*, 75–82.

Streit, J., Tscherter, A., Heuschkel, M.O., and Renaud, P. (2001). The generation of rhythmic activity in dissociated cultures of rat spinal cord. Eur. J. Neurosci. *14*, 191–202.

Tazerart, S., Vinay, L., and Brocard, F. (2008). The persistent sodium current generates pacemaker activities in the central pattern generator for locomotion and regulates the locomotor rhythm. J. Neurosci. *28*, 8577–8589.

Tscherter, A., Heuschkel, M.O., Renaud, P., and Streit, J. (2001). Spatiotemporal characterization of rhythmic activity in rat spinal cord slice cultures. Eur. J. Neurosci. *14*, 179–190.

Van Pelt, J., Corner, M.A., Wolters, P.S., Rutten, W.L., and Ramakers, G.J. (2004). Longterm stability and developmental changes in spontaneous network burst firing patterns in dissociated rat cerebral cortex cell cultures on multielectrode arrays. Neurosci. Lett. *361*, 86–89.

Watanabe, K., Kamiya, D., Nishiyama, A., Katayama, T., Nozaki, S., Kawasaki, H., Watanabe, Y., Mizuseki, K., and Sasai, Y. (2005). Directed differentiation of telencephalic precursors from embryonic stem cells. Nat. Neurosci. *8*, 288–296.

Weick, J.P., Liu, Y., and Zhang, S.C. (2011). Human embryonic stem cell-derived neurons adopt and regulate the activity of an established neural network. Proc. Natl. Acad. Sci. USA *108*, 20189–20194.

Yvon, C., Czarnecki, A., and Streit, J. (2007). Riluzole-induced oscillations in spinal networks. J. Neurophysiol. *97*, 3607–3620.